

Critical dynamics of long-range quantum disordered systems

Weitao Chen ^{1,2,3} Gabriel Lemarié ^{2,3,4,*} and Jiangbin Gong^{1,2,3}

¹*Department of Physics, National University of Singapore, Singapore*

²*MajuLab, Centre National de la Recherche Scientifique–Université Côte d’Azur–Sorbonne Université–National University of Singapore–Nanyang Technological University (CNRS-UCA-SU-NUS-NTU) International Joint Research Unit, Singapore*

³*Centre for Quantum Technologies, National University of Singapore, Singapore*

⁴*Laboratoire de Physique Théorique, Université de Toulouse, Centre National de la Recherche Scientifique, UPS, Toulouse, France*



(Received 6 July 2023; accepted 23 October 2023; published 17 November 2023)

Long-range hoppings in quantum disordered systems are known to yield quantum multifractality, the features of which can go beyond the characteristic properties associated with an Anderson transition. Indeed, critical dynamics of long-range quantum systems can exhibit anomalous dynamical behaviors distinct from those at the Anderson transition in finite dimensions. In this paper, we propose a phenomenological model of wave packet expansion in long-range hopping systems. We consider both their multifractal properties and the algebraic fat tails induced by the long-range hoppings. Using this model, we analytically derive the dynamics of moments and inverse participation ratios of the time-evolving wave packets, in connection with the multifractal dimension of the system. To validate our predictions, we perform numerical simulations of a Floquet model that is analogous to the power law random banded matrix ensemble. Unlike the Anderson transition in finite dimensions, the dynamics of such systems cannot be adequately described by a single parameter scaling law that solely depends on time. Instead, it becomes crucial to establish scaling laws involving both the finite size and the time. Explicit scaling laws for the observables under consideration are presented. Our findings are of considerable interest towards applications in the fields of many-body localization and Anderson localization on random graphs, where long-range effects arise due to the inherent topology of the Hilbert space.

DOI: [10.1103/PhysRevE.108.054127](https://doi.org/10.1103/PhysRevE.108.054127)

I. INTRODUCTION

The study of eigenstate transitions in quantum-disordered systems has attracted a strong interest recently [1]. One celebrated example is the Anderson transition arising from the interplay between interference effects and disorder, which separates a phase where quantum states are localized from a phase where states are delocalized [2–4]. At the Anderson transition, a property called “multifractality” emerges as a consequence of strong and scale invariant spatial fluctuations of the states, intermediate between localization and delocalization [5–7]. Given the importance of the Anderson transition, multifractal properties have been extensively investigated, both theoretically and experimentally, in finite dimensions [8–13] and in random matrix ensembles [14–16]. Recently, it was discovered that quantum multifractality can be observed not only at critical points but also in phases called “extended nonergodic” [17,18]. For example, the many-body localized phase has been shown to have multifractal properties on the Hilbert space [19–21]. The emergence of such nonergodic extended phases has also been described in random matrix ensembles [18,22–31], on the Cayley tree [32–35], in Floquet systems [36–41], in the presence of fractal disorder [42], or in the presence of long-range correlations of disorder [43,44].

Quantum multifractality can be characterized by the moments P_q of order q of eigenstate amplitudes:

$$\langle P_q \rangle = \left\langle \sum_i |\Psi_\alpha(i)|^{2q} \right\rangle \sim N^{-D_q(q-1)}, \quad (1)$$

where the sum is over the N sites (indexed by i) of the system, with the eigenstate amplitudes $|\Psi_\alpha(i)|^2$ normalized as $\sum_i |\Psi_\alpha(i)|^2 = 1$. $\langle \rangle$ denotes an averaging over disorder and eigenstates in a certain energy window. An algebraic scaling of $\langle P_q \rangle$ with N defines a multifractal dimension D_q . $D_q = 1$ indicates an ergodic delocalized behavior, while $D_q = 0$ is a signature of localization. These behaviors are generally observed at a sufficiently large scale, e.g., $N \gg \Lambda$, the correlation or localization volume. Remarkably, $0 < D_q < 1$ indicates scale-invariant multifractal behaviors, the full characterization of which is based on a spectrum of multifractal dimensions [3]. Multifractal eigenstates thus occupy an extensive region which is however an algebraically vanishing fraction of the system: this is why they are called “nonergodic delocalized” [17,18], in contrast to ergodic delocalized states which occupy a finite fraction of the system.

As a characteristic property of the Anderson transition in finite dimensions [9,10,15,45,46], quantum multifractality is even richer in the presence of long-range hoppings. One well-known example is the power-law random banded matrix (PRBM) model [14,15]. Similarly, Floquet models, particularly the Ruijsenaars-Schneider ensemble [47,48], exhibit intriguing properties of quantum multifractality. There,

*lemarie@irsamc.ups-tlse.fr

long-range hoppings introduce anomalous properties beyond typical features at the Anderson transition in finite dimensions. For example, they result in an unusually large critical regime [49], can break a fundamental symmetry of the multifractal spectrum [50], and induce correlation-induced localization [51]. In this paper, we explore how long-range hoppings also give rise to anomalous *dynamical* properties.

In terms of detecting the Anderson transition, solely observing the expansion of a wave packet already serves as a convenient tool. Indeed, this has been extensively studied both theoretically and experimentally [11–13,52–54]. Precisely at the Anderson transition point, the wave packet expansion exhibits an anomalous diffusion behavior that lies between localization and diffusion [11–13,52,54], which needs a more careful quantitative analysis of the wave packet spatial profile to see the impact of multifractality. The expansion dynamics has also been shown to be even more anomalous in quasicrystal systems due to the hierarchical structure of the eigenspectrum [55]. Other observables such as the return probability or the coherent back and forward scattering peaks are more useful to study the multifractal properties of the eigenstates and eigenspectrum [56–64].

Investigation of the quantum dynamics in long-range hopping systems [56–58,60,65–67] in connection with multifractality is more challenging, insofar as the dynamics is strongly affected by the algebraic tails induced by the long-range hoppings (analogous to Lévy flights [67]), as we will show in this paper (see also [28,68]). In particular, the strong boundary effects caused by the algebraic tails present a severe challenge in computational studies. As shown in this paper, it is not possible to circumvent these strong boundary effects by increasing the system size. In other words, one cannot reach a regime where expansion of a wave packet is not affected by finite-size effects, thus requiring more scaling analysis than in the case of the Anderson transition studied both theoretically and experimentally in different platforms [12,13,52,53,63]. Interestingly, in the cases we consider, it is necessary to take into account systematically the boundary effects via a scaling in time, in addition to the system size. Indeed, the focus of this paper is on understanding the subtle critical dynamical behaviors induced by long-range hopping via a two parameter (time and size) scaling approach. Some results were already discussed in Refs. [28,68] using different approaches. This paper distinguishes itself from these studies by providing a coherent description of long-range coupling effects based on a unified model of wave packet propagation in these systems.

Studies of the dynamics of quantum systems are generally computationally expensive. In comparison, simulating the dynamical counterpart of Floquet kicked systems can be made more efficient, as is clear in the kicked rotor dynamics implemented via fast Fourier transforms [69]. Besides their computational efficiency, Floquet kicked systems also exhibit rich dynamical behaviors such as dynamical localization [70,71], or Floquet time crystals [72]. In this paper, we employ a Floquet kicked model with algebraically long-range hoppings and eigenstates with multifractal properties [73] to simulate numerically the critical dynamics in such long-range hopping systems. We propose scaling laws the scaling parameters of which include both time and system size, for different observables, based on a general and simple phenomenological

model of wave packet expansion in the type of systems considered. Our analytical and numerical results demonstrate distinct dynamical behaviors depending on the observables considered.

As an outlook, we note that algebraic fat tails in time evolving wave packets are also relevant to studies of quantum dynamics on various graphs of infinite effective dimension, such as Anderson localization in random graphs [50,74,75] or the Hilbert space of a many-body localized system [76–78]. The Hilbert spaces of these systems have network structure where the number N_r of sites at distance r from the localization center of a wave packet grows exponentially, therefore the exponential decay of the wave packet with distance r can be regarded as an algebraic behavior as a function of N_r . Under the new coordinate N_r , important localization measures like the inverse participation ratio can be more easily studied since the network structure is simplified to one dimension. Hence, our findings hold potential relevance in this context, which has recently gathered significant attention.

The rest of the paper is organized as follows. In Sec. II, we introduce the kicked Floquet model we consider and discuss its multifractal properties. In Sec. III, we recall the temporal behavior and finite-size dependence of the return probability $\langle R_0 \rangle$ and generalize these known results to higher moments $\langle R_0^q(t) \rangle$. In Sec. IV, we propose a general phenomenological model of wave packet expansion in long-range hopping systems with multifractal properties, based on both analytical arguments and numerical observations. In Sec. V, we derive from the phenomenological model the dynamics and time and size scaling laws for two other important types of observables (some may be accessible experimentally): the average k th moments of a wave packet $\langle p^k \rangle$ and the q th inverse participation ratio $\langle P_q(t) \rangle$. We present numerical results that validate our predictions. We conclude our paper in Sec. VI.

II. THE MULTIFRACTAL KICKED ROTOR MODEL

In this paper, we investigate a variant of the quantum kicked rotor [70,71] that we call the “multifractal kicked rotor” (MKR) model, with Hamiltonian [73]

$$\mathcal{H} = \frac{p^2}{2} + KV(q) \sum_n \delta(t - nT), \quad (2)$$

where

$$V(q) = \begin{cases} \ln(q/\pi), & q \in [0, \pi), \\ \ln(2 - q/\pi), & q \in [\pi, 2\pi), \end{cases} \quad (3)$$

and $V(q + 2\pi) = V(q)$, the Floquet period T of which is set to be $T = 1$ in the rest of the paper. Hamiltonian Eq. (2) yields a Floquet operator $U = \exp(-p^2/2\hbar) \exp[-iKV(q)/\hbar]$, which can be quantized in a truncated Hilbert space with dimension N with $p = P\hbar$, with P an integer between $-\frac{N}{2}$ and $\frac{N}{2} - 1$, and $q = \frac{2\pi Q - \varepsilon}{N}$, with Q an integer between 1 and N satisfying periodic boundary conditions in both P and Q .

However, note that we have assigned the value of $\varepsilon = 1$ for $q \in [\pi, 2\pi)$ (i.e., when $Q = 1, \dots, \frac{N}{2}$), while for other values of q we have set $\varepsilon = 0$ to prevent numerical divergence. These slight shifts disrupt the symmetry of the kicking potential in Eq. (3) around the axis $q = \pi$. The conventional time-reversal symmetry is typically defined as $t \rightarrow -t$, $q \rightarrow q$,

and $p \rightarrow -p$ when analyzing the transport properties of wave packets in the q space (which we denote as the direct space). In this context, the transformation $p \rightarrow -p$ represents an inversion in the reciprocal space. In the case of kicked systems, where the emphasis is on the transport properties in the momentum space (p space), the reciprocal space becomes the q space, and the standard momentum inversion associated with time-reversal symmetry in Hamiltonian systems is modified to spatial inversion. Hence, the adapted definition of time-reversal symmetry for kicked systems is typically expressed as $t \rightarrow -t$, $q \rightarrow -q$, and $p \rightarrow p$ (see [79,80]). However, in our system, q is defined in the range $[0, 2\pi)$, requiring a modification of spatial inversion to $q \rightarrow q - \pi$. This alteration differs from the conventional spatial inversion ($q \rightarrow -q$) only by a trivial global phase factor. Consequently, the asymmetry introduced in the kicking potential $V(q)$ breaks the transformation $q \rightarrow q - \pi$, thereby breaking the time-reversal symmetry of the Hamiltonian.

The phases corresponding to the kinetic energy $\Phi_p \equiv P^2 \hbar / 2$ are pseudorandom phases when \hbar is irrational with 2π [81–83]. Here, we consider Φ_p as fully random phases, uniformly distributed over $[0, 2\pi)$. In our numerical simulations, disorder averaging is performed over various configurations of these random phases. Without loss of generality, we set $\hbar = 1$ in the rest of the paper. We can therefore treat p and P as the same variable, and we will no longer use the notation P in the following.

The Floquet operator can be explicitly expressed in the momentum space using a discrete Fourier transform as

$$U_{pp'} = e^{-i\Phi_p} \sum_{Q=1}^N F_{pQ} e^{-iKV(2\pi Q/N)} F_{Qp'}^{-1}, \quad (4)$$

where $F_{pQ} = \frac{1}{\sqrt{N}} e^{2i\pi pQ/N}$. Due to the singular behavior of $V(q)$ when $q \rightarrow 0$ (2π), the amplitudes of the matrix elements of $U_{pp'}$ decay as

$$|U_{pp'}| \sim \frac{1}{|p - p'|} \quad (5)$$

for large $|p - p'|$ (note that there is another higher-order singularity at $q = \pi$ which can be neglected; see [73] and Appendix A for more details). In Appendix B, we characterize the multifractal properties of the MKR model, and in particular extract the multifractal dimension $D_2 = 0.71$ for $K = 10$ by analyzing the system size dependence of eigenstate moments numerically. Another Floquet system, the Ruijsenaars-Schneider model with similar long-range hopping amplitudes, has been extensively studied for its multifractal properties [48], spectral statistics [84], and rich dynamics [66]. Additionally, it is worth noting that by generalizing the kicking potential $V(q)$ of the MKR model to $V(q) = |q|^\beta$, the model hosts delocalized eigenstates for $\beta < 0$ and localized eigenstates for $\beta > 0$ (see [73]). The potential $V(q)$ chosen in this paper corresponds to the limit as $\beta \rightarrow 0$, i.e., the critical case.

III. RETURN PROBABILITY R_0

Before describing the behavior of observables which are significantly affected by the long-range hoppings introduced

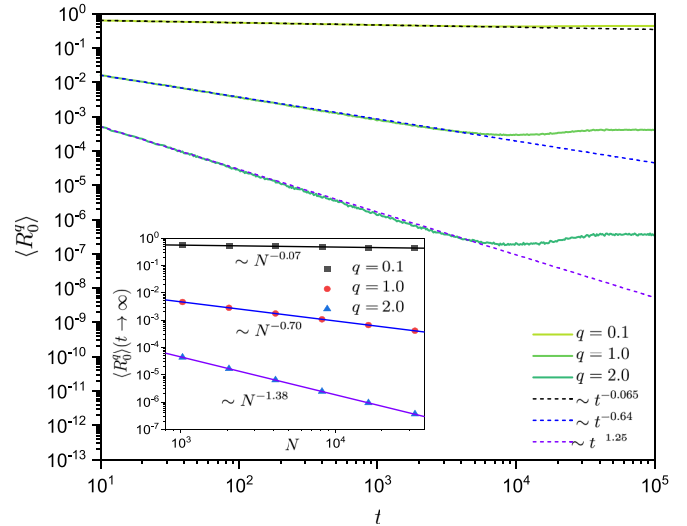


FIG. 1. Dynamics of $\langle R_0^q \rangle$ in the MKR model Eq. (2) for $K = 10$ and $q = 0.1, 1.0$, and 2.0 from top to bottom. The dashed lines indicate fits with an algebraic law, validating Eq. (6) for $t < t_N^*$ with $D_2^\mu = 0.64$. The system size is $N = 2^{15}$. Inset: Finite-size scaling of saturation values of $\langle R_0^q(t \rightarrow \infty) \rangle$, verifying Eq. (7) for $t > t_N^*$ with $D_2^\psi = 0.70$. The multifractal dimensions $D_2^\mu \approx D_2^\psi \approx D_2 = 0.71$, as expected for this type of system [60]. Numerical results have been averaged over 4800 random phase configurations.

above, we recall the properties of a dynamical observable, the return probability R_0 , which has been extensively investigated as a characteristic signature of quantum multifractality [57,58,63,85,86]. Starting from an initial condition $\psi(p, t = 0) = \delta_{p,0}$, R_0 is defined as $R_0 \equiv |\psi(p = 0, t)|^2$. As a result of multifractal properties, R_0 decays as a power law with time, $\langle R_0 \rangle \sim t^{-D_2^\mu}$ where D_2^μ is the multifractal dimension of the spectral measure (see [56–58,60,87] and Appendix C).

In our paper, higher moments $\langle R_0^q \rangle$ with $q > 0$ will play a key role. Due to narrow distributions of large wave function amplitudes $|\psi|^2$ in such systems (see [50] and Appendix E), the power-law decay of $\langle R_0 \rangle$ can be simply generalized to $\langle R_0^q \rangle$ with $q > 0$ as

$$\langle R_0^q \rangle \sim t^{-qD_2^\mu}, \quad (6)$$

as illustrated in Fig. 1.

On the other hand, in a finite system of size N , there exists a characteristic time scale t_N^* after which R_0 reaches a finite stationary value, equal to the inverse participation ratio $\langle P_2 \rangle$ [Eq. (1)], i.e., $\langle R_0(t \rightarrow \infty) \rangle = \langle P_2 \rangle \sim N^{-D_2^\psi}$, where D_2^ψ is the spatial multifractal dimension of the eigenstates [65,68]. Similarly, we find that the size dependence of $\langle R_0^q \rangle$ at large times follows:

$$\langle R_0^q(t \rightarrow \infty) \rangle \sim N^{-qD_2^\psi}. \quad (7)$$

Therefore, the characteristic time t_N^* should scale as

$$t_N^* \sim N^{D_2^\psi/D_2^\mu}. \quad (8)$$

t_N^* reduces to the Heisenberg time (inverse of the mean level spacing $2\pi/N$) for systems with $D_2^\psi = D_2^\mu$ [57–59]. Combining the above relations, we can infer the following two

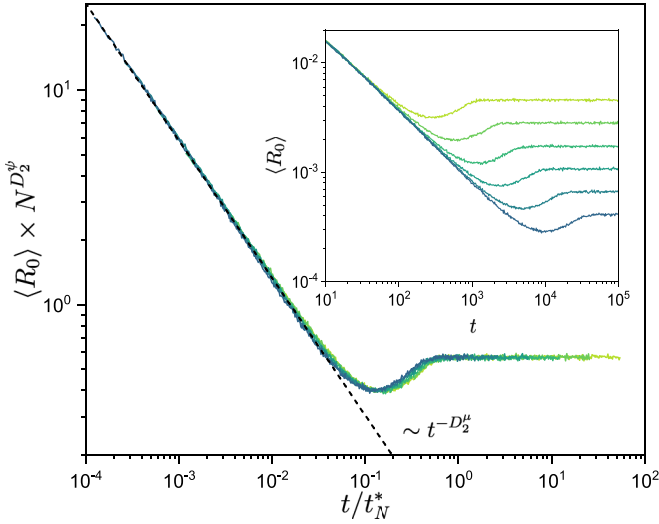


FIG. 2. Demonstration of the scaling property Eq. (9) for the return probability R_0 in the MKR model Eq. (2): the data corresponding to different system sizes $N = 2^{10}, 2^{11}, \dots, 2^{15}$ and different times $t \in [10, 10^5]$ all collapse onto a single scaling curve when $\langle R_0 \rangle \times N^{D_2^\psi}$ is plotted as a function of the scaled time t/t_N^* . The dashed line indicates a fit by the power law $\langle R_0 \rangle \sim t^{-D_2^\mu}$ with $D_2^\mu \approx 0.64$. Inset: Corresponding raw data $\langle R_0 \rangle$. Curves from top to bottom correspond to system sizes $N = 2^{10}, 2^{11}, \dots, 2^{15}$, respectively. Results have been averaged over 4800 disorder configurations with the kicked strength $K = 10$.

parameter scaling behavior for R_0 :

$$\langle R_0^q(t, N) \rangle = N^{-qD_2^\psi} g(t/t_N^*). \quad (9)$$

The numerical data for the MKR verify the above scaling relations. Results presented in Fig. 1 validate Eqs. (6) and (7). By fitting the corresponding data, we extract the multifractal dimensions $D_2^\mu = 0.64$ and $D_2^\psi = 0.70$. In Fig. 2, the collapse of R_0 onto a single scaling curve when $\langle R_0 \rangle N^{D_2^\psi}$ is plotted as a function of t/t_N^* confirms the validity of the proposed scaling law Eq. (9). In Appendix D, we show similar scaling properties for $\langle R_0^q \rangle$ with $q = 0.1$ and 2. Similar scaling properties for $\langle R_0 \rangle$ (i.e., $q = 1$) have been observed in [59] in both single-particle and many-body quantum systems. It is worth noting that there are other dynamical observables that can detect multifractality with dimensions other than D_2 . For instance, the coherent forward scattering peak, the dynamics of which is also governed by the information dimension D_1 , has been explored [62,64].

IV. PHENOMENOLOGICAL MODEL FOR THE EXPANSION OF A WAVE PACKET IN MULTIFRACTAL SYSTEMS WITH ALGEBRAIC LONG-RANGE HOPPINGS

We shall now describe the rich and subtle effects of algebraic long-range hoppings on the critical dynamics of a wave packet, effects that cannot be characterized using the widely used return probability. We construct in this section a phenomenological model, based on known analytical results and simple arguments such as wave packet normalization, and validate this model by numerical simulations using the MKR

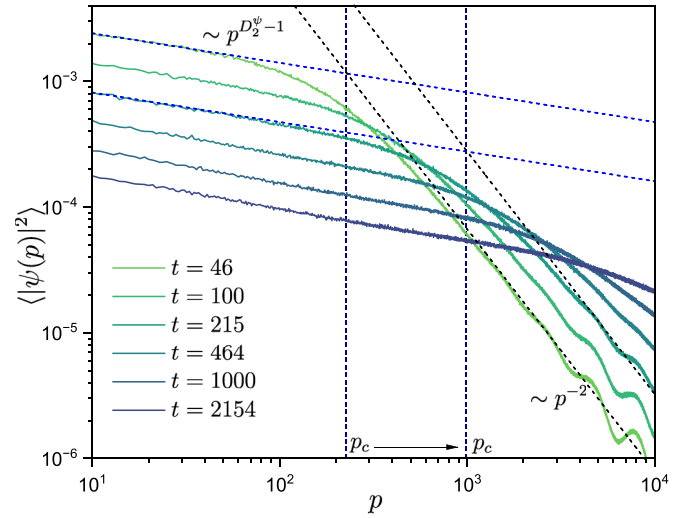


FIG. 3. Average probability distribution of wave packets $\langle |\psi(p, t)|^2 \rangle$ at different times for the MKR model with initial condition $\psi(p, t=0) = \delta_{p,0}$. The dashed lines show the two power-law behaviors corresponding to Eq. (10) and the multifractal wavefront p_c . Results have been averaged over 4800 disorder configurations with the kicked strength $K = 10$ for system size $N = 2^{15}$.

model Eq. (2). Here we restrict our analysis to the regime $p > 0$, since we expect similar scaling behavior for $p < 0$, as the wave packet is initialized as $\psi(p, t=0) = \delta_{p,0}$.

Starting from a wave packet initialized at a single site $p = 0$, long-range hoppings will induce a power-law tail of the wave packet. This tail is primarily determined by the hopping elements before any interference effects induced by multifractality occur. If the long-range hoppings follow the behavior described in Eq. (5), then the tail of the wave packet behaves as $\langle |\psi(p)|^2 \rangle \sim p^{-2}$, the so-called Lévy flight tail [67]. However, in the vicinity of the site $p = 0$ where the wave packet was initialized, a nontrivial power-law decay $\langle |\psi(p)|^2 \rangle \sim p^{D_2^\psi - 1}$ dynamically emerges, which is controlled by the spatial correlation dimension D_2^ψ of the wave function [63,65,67,86].

Figure 3 represents the averaged probability distribution of a wave packet initialized at $p = 0$, $\langle |\psi(p, t)|^2 \rangle$ at different times, for the MKR model Eq. (2). Two distinct power-law decays with p are clearly visible: a fast decay $\langle |\psi(p, t)|^2 \rangle \sim p^{-2}$ at large $p \gg p_c$, and a slower decay $\langle |\psi(p, t)|^2 \rangle \sim p^{D_2^\psi - 1}$ close to the initial condition $p \ll p_c$. The crossover scale p_c has a nontrivial dependence on time which we will describe in the following. It is equivalent to the characteristic scale mentioned in [85,86], which distinguishes the scaling behaviors of the density correlation function in the position-frequency representation, specifically between the large and small position regimes. Crucially for our paper, we also observe that other moments of wave packet amplitudes, $\langle |\psi(p, t)|^{2q} \rangle$ with $q > 0$, obey a similar behavior [see Eq. (10)]. The distributions for different q thus share the same shape, in particular the same p_c (see Appendix E for more details).

Based on these observations, we propose the following phenomenological model for the average probability distributions of the generalized wave packets $\langle |\psi(p, t)|^{2q} \rangle$

TABLE I. Summary of the analytical predictions of the finite-time and finite-size dependence of the dynamics of the k th moments $\langle p^k \rangle$ and q th inverse participation ratios $\langle P_q(t) \rangle$.

Observable	$\langle p^k \rangle$		$\langle P_q \rangle$		
	$k < \lambda - 1$	$k > \lambda - 1$	$0 < q < \frac{1}{\lambda}$	$\frac{1}{\lambda} < q < \frac{1}{1-D_2^\psi}$	$q > \frac{1}{1-D_2^\psi}$
Finite-time dependence	$t^{k(D_2^\mu/D_2^\psi)}$	$t^{(\lambda-1)D_2^\mu/D_2^\psi}$	$t^{q(\lambda-1)D_2^\mu/D_2^\psi}$	$t^{(1-q)D_2^\mu/D_2^\psi}$	$t^{-qD_2^\mu}$
Finite-size dependence	N^k	N^k	N^{1-q}	N^{1-q}	$N^{-qD_2^\psi}$
Scaling law	$N^k g(t/t_N^*)$		$N^{1-q} g(t/t_N^*)$		$N^{-qD_2^\psi} g(t/t_N^*)$

for $q > 0$:

$$\langle |\psi(p, t)|^{2q} \rangle = \begin{cases} \langle R_0^q \rangle p^{-q\mu}, & 1 \leq p < p_c, \\ B \left[\frac{p}{p_c} \right]^{-q\lambda}, & p_c < p \leq \frac{N}{2}, \end{cases} \quad (10)$$

where λ is the exponent of the power-law tail at large $p \gg p_c$ ($\lambda = 2$ in the MKR model), $\mu = 1 - D_2^\psi$ is the exponent of the power law decay at small $p \ll p_c$, related to the multifractal dimension D_2^ψ , and $B = \langle R_0^q \rangle [p_c]^{-q\mu}$. Note that our model is valid only above a microscopic cutoff taken as $p_{\min} = 1$ here. This cutoff usually corresponds to the mean free path (see, e.g., [63]). In the following, we will neglect contributions below this cutoff, which are not of our interest here.

The crossover scale p_c between the two power-law regimes can be interpreted as a multifractal wavefront. Its dynamics and finite-size scaling play an important role in the following. They can be understood simply by invoking normalization of the wave packet $\langle |\psi|^2 \rangle \equiv \sum_{p=-\frac{N}{2}}^{\frac{N}{2}-1} |\psi(p, t)|^2 \simeq 2 \int_1^{\frac{N}{2}} |\psi(p, t)|^2 dp$, where we have taken into account the fact that the wave packet is symmetric with respect to the origin and neglected contributions below the cutoff $p < 1$. Therefore,

$$\begin{aligned} 1 &= \langle |\psi|^2 \rangle \simeq 2 \left[\int_1^{p_c} \langle R_0 \rangle p^{-\mu} dp + \int_{p_c}^{\frac{N}{2}} B \left(\frac{p}{p_c} \right)^{-\lambda} dp \right] \\ &= \frac{2\langle R_0 \rangle}{1-\mu} (p_c^{1-\mu} - 1) \\ &\quad + \frac{2\langle R_0 \rangle p_c^{-\mu}}{1-\lambda} \left[p_c^\lambda \left(\frac{N}{2} \right)^{1-\lambda} - p_c \right]. \end{aligned} \quad (11)$$

The previous expression can be simplified, using $\mu = 1 - D_2^\psi$, as

$$\begin{aligned} &\left(\frac{1}{D_2^\psi} + \frac{1}{\lambda-1} \right) p_c^{D_2^\psi} - \frac{1}{\lambda-1} p_c^{\lambda+D_2^\psi-1} \left(\frac{N}{2} \right)^{1-\lambda} \\ &\simeq \frac{1}{2\langle R_0 \rangle} + \frac{1}{D_2^\psi}. \end{aligned} \quad (12)$$

The second term in the left-hand side of the above equality vanishes when $N \rightarrow \infty$ if $\lambda > 1$, as is the case in the MKR model considered. Using $\langle R_0 \rangle \sim t^{-D_2^\mu}$ for $t < t_N^*$ [Eq. (8)], we get the following dynamical behavior

of p_c :

$$p_c \sim t^{\frac{D_2^\mu}{D_2^\psi}}, \quad (t \ll t_N^*). \quad (13)$$

In the limit of large times $t \gg t_N^*$, substituting $R_0(t \rightarrow \infty) = P_2 \sim N^{-D_2^\psi}$, one gets

$$p_c(t \rightarrow \infty) \sim N. \quad (t \gg t_N^*). \quad (14)$$

As said above, we have shown in Appendix E that the multifractal wavefront p_c is the same for generalized wave packets $\langle |\psi(p, t)|^{2q} \rangle$ with different q . Moreover, we anticipate that our wave packet descriptions are not bound by specific models, as our reasoning relies solely on two fundamental properties of the system: multifractality and long-range hoppings. In Appendix F, we present the averaged probability distribution of wave packets for the PRBM model [14,15].

V. TWO PARAMETER SCALING IN SIZE AND TIME FOR CRITICAL QUANTUM DYNAMICS OF ALGEBRAICALLY LONG-RANGE SYSTEMS

In this section, we employ the phenomenological model introduced in Eq. (10) to derive the critical dynamics dependent on time and size, in terms of the average k th moments of a wave packet $\langle p^k \rangle$. The observation of $\langle p^k \rangle$ is possible in cold atom systems [11,13] and ultrasound experiments [9], thus making it an experimentally accessible observable. Furthermore, we examine the q th inverse participation ratio $\langle P_q(t) \rangle$, which is a significant quantity in standard multifractal analysis (see [66] for more information). Based on these dynamical observables, we propose scaling laws that are dependent on both time and size. In Table I, we summarize the analytical predictions of the finite-time and size-dependent dynamics for both observables. The MKR model of Eq. (2) is used to numerically verify the predicted critical dynamics and their respective scaling laws.

A. k th moment $\langle p^k \rangle$ of a wave packet

The average k th moments of a wave packet $\langle p^k \rangle$

$$\langle p^k \rangle = \sum_{p=-\frac{N}{2}}^{\frac{N}{2}-1} |p|^k \langle |\psi(p, t)|^2 \rangle \quad (15)$$

reflect the diffusive properties of a system. Note that we have defined the moments using an absolute value of p since the wave packet is symmetric with respect to the origin $p = 0$.

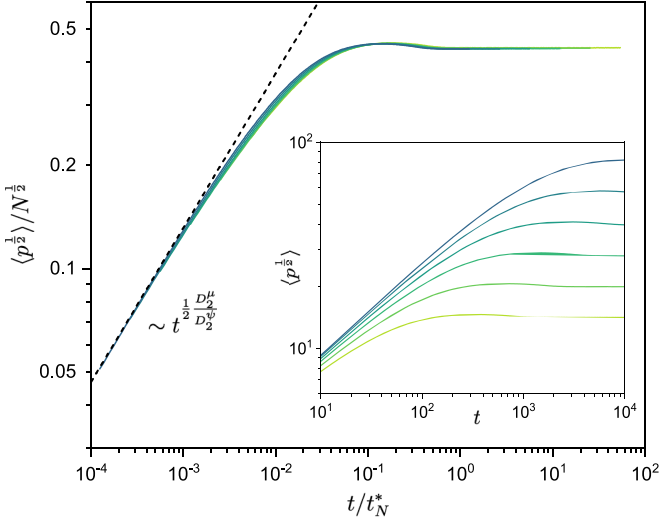


FIG. 4. Demonstration of the scaling property Eq. (19) for the moment of the wave packet $\langle p^{\frac{1}{2}} \rangle$ in the MKR model Eq. (2): the data corresponding to different system sizes $N = 2^{10}, 2^{11}, \dots, 2^{15}$ and different times $t \in [10, 10^5]$ all collapse onto a single scaling curve when $\langle p^{\frac{1}{2}} \rangle / N^{\frac{1}{2}}$ is plotted as a function of the scaled time t/t_N^* . The dashed line indicates a fit by the power law $\langle p^{\frac{1}{2}} \rangle \sim t^{\frac{1}{2} \frac{D_2^\mu}{D_2^\psi}}$. Inset: Corresponding raw data $\langle p^{\frac{1}{2}} \rangle$. Curves from top to bottom correspond to system sizes $N = 2^{10}, 2^{11}, \dots, 2^{15}$, respectively. Results have been averaged over 4800 disorder configurations with the kicked strength $K = 10$.

Based on the phenomenological model proposed in Eq. (10),

$$\begin{aligned} \langle p^k \rangle &\approx 2 \int_1^{\frac{N}{2}} |\psi(p, t)|^2 p^k dp \\ &= \int_1^{p_c} 2 \langle R_0 \rangle p^{k-\mu} dp + \int_{p_c}^{\frac{N}{2}} 2B p_c^\lambda p^{k-\lambda} dp \\ &= \frac{2 \langle R_0 \rangle}{k+1-\mu} (p_c^{k+1-\mu} - 1) \\ &\quad + \frac{2 \langle R_0 \rangle}{k+1-\lambda} \left[p_c^{\lambda-\mu} \left(\frac{N}{2} \right)^{k+1-\lambda} - p_c^{k+1-\mu} \right]. \end{aligned} \quad (16)$$

Combining the time-dependent analysis of p_c and $\langle R_0 \rangle$ in Eq. (16), the time-dependent dynamics of $\langle p^k \rangle$ can be derived as

$$\begin{aligned} \langle p^k \rangle &\sim \langle R_0 \rangle p_c^{k+1-\mu} + \langle R_0 \rangle p_c^{\lambda-\mu} N^{k+1-\lambda} \\ &\sim t^{\frac{k}{2} \frac{D_2^\mu}{D_2^\psi}} + t^{(\lambda-1) \frac{D_2^\mu}{D_2^\psi}} N^{k+1-\lambda}, \end{aligned} \quad (17)$$

for $t \ll t_N^*$.

For $k < \lambda - 1$, the second term of Eq. (17) vanishes when $N \rightarrow \infty$, yielding $\langle p^k \rangle \sim t^{k \frac{D_2^\mu}{D_2^\psi}}$. This regime was previously investigated in the Fibonacci chain and Harper model in [65]. Nevertheless, for $k > \lambda - 1$, the second term dominates, contributing $\langle p^k \rangle \sim t^{(\lambda-1) \frac{D_2^\mu}{D_2^\psi}}$. For the MKR model, the power-law tail exponent $\lambda = 2$, which yields $\langle p^k \rangle \sim t^{D_2^\mu/D_2^\psi}$ for $k > 1$ and $\langle p^k \rangle \sim t^{k D_2^\mu/D_2^\psi}$ for $0 < k < 1$. The numerical results shown in Figs. 4 and 5 confirm such predictions. The

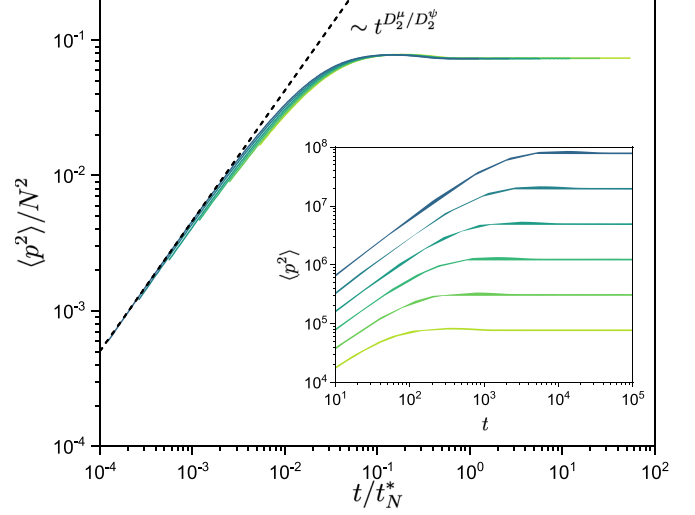


FIG. 5. Demonstration of the scaling property Eq. (19) for the moment of the wave packet $\langle p^2 \rangle$ in the MKR model Eq. (2): the data corresponding to different system sizes $N = 2^{10}, 2^{11}, \dots, 2^{15}$ and different times $t \in [10, 10^5]$ all collapse onto a single scaling curve when $\langle p^2 \rangle / N^2$ is plotted as a function of the scaled time t/t_N^* . The dashed line indicates a fit by the power law $\langle p^2 \rangle \sim t^{D_2^\mu/D_2^\psi}$. Inset: Corresponding raw data $\langle p^2 \rangle$. Curves from top to bottom correspond to system sizes $N = 2^{10}, 2^{11}, \dots, 2^{15}$, respectively. Results have been averaged over 4800 disorder configurations with the kicked strength $K = 10$.

diffusive exponents for $\langle p^k \rangle$ are independent of k when $k > \lambda - 1$, which is a nontrivial consequence of the power-law tail of the wave packet induced by algebraic long-range hoppings.

Furthermore, using the finite-size scaling of $p_c \sim N$ and $R_0 \sim N^{-D_2^\psi}$ at large $t \gg t_N^*$, we can also derive the finite-size scaling of $\langle p^k \rangle$:

$$\langle p^k(t \rightarrow \infty) \rangle \sim N^k. \quad (18)$$

Finally, a two parameter scaling law for $\langle p^k \rangle$ can be naturally proposed based on the time dependence of Eq. (17) and the finite-size dependence of Eq. (18):

$$\langle p^k(t, N) \rangle = N^k g(t/t_N^*). \quad (19)$$

The presented numerical results in Figs. 4 and 5 demonstrate that the data for $\langle p^2 \rangle$ of the MKR model adhere to the proposed scaling behavior. The data collapse onto a single scaling curve when $\langle p^2 \rangle / N^2$ is plotted as a function of t/t_N^* . Additionally, in Appendix D, we provide numerical data for $\langle p^3 \rangle$ and $\langle p^5 \rangle$, which confirm the validity of the aforementioned predictions.

B. q th inverse participation ratio $\langle P_q(t) \rangle$ of a wave packet

We now turn to another key observable for multifractal properties, the generalized inverse participation ratios. As we are interested in the dynamics of a wave packet, we do not consider the $\langle P_q \rangle$ of the eigenstates [Eq. (1)], but the $\langle P_q(t) \rangle$ of the time-evolving wave packet at a certain instant t :

$$\langle P_q(t) \rangle \equiv \left\langle \sum_{p=-\frac{N}{2}}^{p=\frac{N}{2}-1} |\psi(p, t)|^{2q} \right\rangle. \quad (20)$$

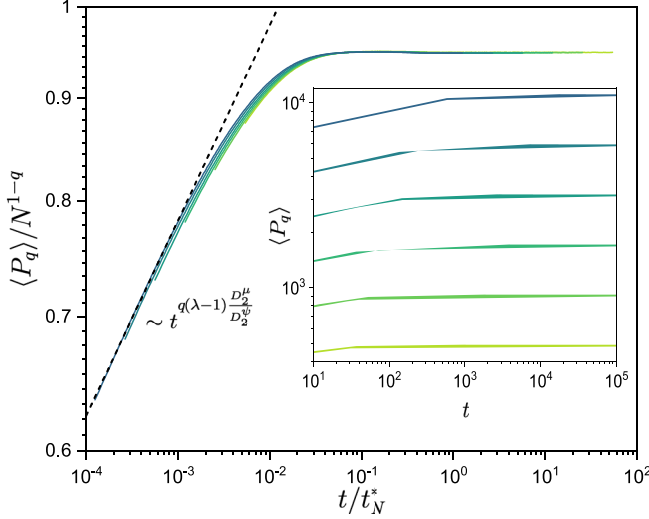


FIG. 6. Demonstration of the scaling property Eq. (25) for $\langle P_q \rangle$ in the MKR model Eq. (2) when $q = 0.1$: the data corresponding to different system sizes $N = 2^{10}, 2^{11}, \dots, 2^{15}$ and different times $t \in [10, 10^5]$ all collapse onto a single scaling curve when $\langle P_q \rangle / N^{1-q}$ is plotted as a function of the scaled time t/t_N^* . The dashed line indicates a fit by the power law $\langle P_q \rangle \sim t^{q(\lambda-1)D_2^\mu/D_2^\psi}$. Inset: Corresponding raw data $\langle P_q \rangle$. Curves from top to bottom correspond to system sizes $N = 2^{10}, 2^{11}, \dots, 2^{15}$, respectively. Results have been averaged over 4800 disorder configurations with the kicked strength $K = 10$.

We will study how $\langle P_q(t) \rangle$ scales with system size, but also characterize its temporal behavior. The scaling with system size of the moments $\langle P_q \rangle$ of eigenstates captures the multifractality of critical systems directly, exhibiting distinct algebraic behaviors for different values of q . By contrast, the moments $\langle P_q(t) \rangle$ for a time-evolving wave packet are different as they are nonequilibrium observables capturing the dynamical growth of the participation volume of the eigenstate (e.g., $\langle P_2(t) \rangle$ being the inverse volume occupied by the wave packet).

Similar to the analysis of the average k th moments $\langle p^k \rangle$, $\langle P_q(t) \rangle$ can be calculated as

$$\begin{aligned} \langle P_q(t) \rangle &= 2 \int_1^{\frac{N}{2}} \langle |\psi(p, t)|^{2q} \rangle dp \\ &= \int_1^{p_c} 2 \langle R_0^q \rangle p^{-q\mu} dp + \int_{p_c}^{\frac{N}{2}} 2B^q p_c^{q\lambda} p^{-q\lambda} dp \\ &= \frac{2 \langle R_0^q \rangle}{1 - q\mu} (p_c^{1-q\mu} - 1) \\ &\quad + \frac{2 \langle R_0^q \rangle}{1 - q\lambda} \left[p_c^{q(\lambda-\mu)} \left(\frac{N}{2} \right)^{1-q\lambda} - p_c^{1-q\mu} \right] \\ &\sim t^{(1-q) \frac{D_2^\mu}{D_2^\psi}} + t^{q(\lambda-1) \frac{D_2^\mu}{D_2^\psi}} N^{1-q\lambda}. \end{aligned} \quad (21)$$

When $N \rightarrow \infty$, for $q > 1/\lambda$, i.e., $q > \frac{1}{2}$ for $\lambda = 2$, the second term of the right hand side of Eq. (21) vanishes, yielding the time-dependent decay $\langle P_q \rangle \sim t^{(1-q)D_2^\mu/D_2^\psi}$. Otherwise, for $q < 1/\lambda$, i.e., $q < \frac{1}{2}$ for $\lambda = 2$, the second term dominates, resulting in a time-dependent increase $\langle P_q \rangle \sim t^{q(\lambda-1)D_2^\mu/D_2^\psi}$.

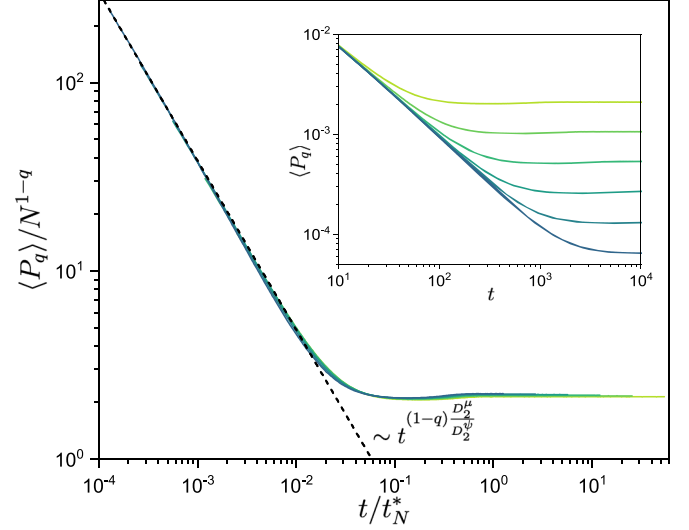


FIG. 7. Demonstration of the scaling property Eq. (25) for $\langle P_q \rangle$ in the MKR model Eq. (2) when $q = 2$: the data corresponding to different system sizes $N = 2^{10}, 2^{11}, \dots, 2^{15}$ and different times $t \in [10, 10^5]$ all collapse onto a single scaling curve when $\langle P_q \rangle / N^{1-q}$ is plotted as a function of the scaled time t/t_N^* . The dashed line indicates a fit by the power law $\langle P_q \rangle \sim t^{(1-q)D_2^\mu/D_2^\psi}$. Inset: Corresponding raw data $\langle P_q \rangle$. Curves from top to bottom correspond to system sizes $N = 2^{10}, 2^{11}, \dots, 2^{15}$, respectively. Results have been averaged over 4800 disorder configurations with the kicked strength $K = 10$.

Applying a similar analysis for the finite-size saturation value at $t \gg t_N^*$ yields

$$\langle P_q(t \rightarrow \infty) \rangle \sim N^{-qD_2^\psi} N^{1-q\mu} \sim N^{1-q}. \quad (22)$$

However, Eq. (21) is valid only if $p_c^{1-q\mu} - 1 > 0$, i.e., $q < \frac{1}{1-D_2^\psi}$. If $q > \frac{1}{1-D_2^\psi}$, the contribution of the multifractal wavefront in the integral is smaller than or close to 1. The term $\frac{\langle R_0^q \rangle}{1-q\mu} (p_c^{1-q\mu} - 1)$ is then dominated by $\langle R_0^q \rangle$, yielding

$$\begin{aligned} \langle P_q \rangle &\simeq \frac{2 \langle R_0^q \rangle}{1 - q\mu} + \frac{2 \langle R_0^q \rangle}{1 - q\lambda} p_c^{q(\lambda-\mu)} \left(\frac{N}{2} \right)^{1-q\lambda} \\ &\sim t^{-qD_2^\mu} + t^{q(\lambda-1) \frac{D_2^\mu}{D_2^\psi}} N^{1-q\lambda}, \end{aligned} \quad (23)$$

and

$$\langle P_q(t \rightarrow \infty) \rangle \sim N^{-qD_2^\psi}. \quad (24)$$

Equation (23) shows another regime where $\langle P_q \rangle \sim t^{-qD_2^\mu}$ when $q > \frac{1}{1-D_2^\psi}$ and $1/\lambda$. Combining the derivations above, two scaling laws can be proposed as

$$\begin{aligned} \langle P_q(t, N) \rangle &= N^{1-q} g(t/t_N^*), \quad 0 < q < \frac{1}{1 - D_2^\psi}, \\ \langle P_q(t, N) \rangle &= N^{-qD_2^\psi} g(t/t_N^*), \quad q > \frac{1}{1 - D_2^\psi}. \end{aligned} \quad (25)$$

Applying the above insights to the MKR model considered here, overall it is clear that there are three regimes where P_q varies with distinct exponents. For $q < 0.5$, $\langle P_q \rangle \sim t^{q(\lambda-1)D_2^\mu/D_2^\psi}$; for $0.5 < q < \frac{1}{1-D_2^\psi} \approx 3.3$, $\langle P_q \rangle \sim t^{(1-q)D_2^\mu/D_2^\psi}$;

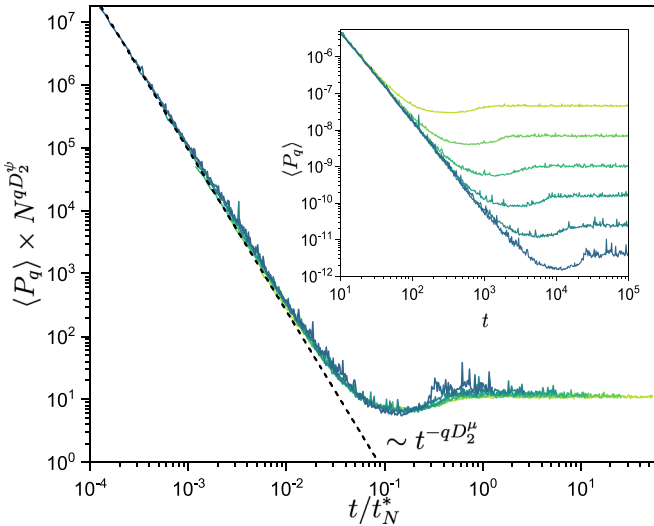


FIG. 8. Demonstration of the scaling property Eq. (25) for $\langle P_q \rangle$ in the MKR model Eq. (2) when $q = 4$: the data corresponding to different system sizes $N = 2^{10}, 2^{11}, \dots, 2^{15}$ and different times $t \in [10, 10^5]$ all collapse onto a single scaling curve when $\langle P_q \rangle / N^{1-q}$ is plotted as a function of the scaled time t/t_N^* . The dashed line indicates a fit by the power law $\langle P_q \rangle \sim t^{-qD_2^\mu}$. Inset: Corresponding raw data $\langle P_q \rangle$. Curves from top to bottom correspond to system sizes $N = 2^{10}, 2^{11}, \dots, 2^{15}$, respectively. Results have been averaged over 4800 disorder configurations with the kicked strength $K = 10$.

and for $q > \frac{1}{1-D_2^\mu}$, $\langle P_q \rangle \sim t^{-qD_2^\mu}$. Figures 6–8 present the collapse of data for $q = 0.1, 2$, and 4 , corresponding to the three distinct dynamical regimes. The different dynamical exponents are in good agreement with the predictions, and the collapse of the rescaled data confirms the validity of the proposed scaling laws; similar numerical observations are also reported in [68] with the power-law banded Anderson model.

VI. CONCLUSION

In conclusion, we have presented a thorough investigation into the wave packet dynamics of disordered quantum critical systems, exploring the anomalous effects of long-range hoppings in the presence of multifractal properties eigenstates. Our paper indicates that long-range hoppings can induce subtle and rich dynamical behaviors. For example, the wave packet variance may increase linearly with time, namely, $\langle p^2 \rangle \sim t$, which could be akin to a diffusive behavior [28] though the system is multifractal. The multifractal properties of the wave packet dynamics itself, as characterized by the $\langle P_q(t) \rangle$, are all related to the fractal dimension D_2 , but, according to the value of q , can have different scaling behaviors on system size N and time t .

Algebraic tails of time-evolving wave packets appear generically in systems with long-range couplings, but also effectively in localization problems on graphs of infinite dimensionality, such as in many-body localization. For these systems, this paper indicates that we cannot avoid finite-size effects, and that these effects can be taken into account via a two parameter scaling theory depending on time t and the system size N .

It would be interesting to extend our study to either delocalized or localized phases of disordered systems with long-range hoppings, where the couplings decrease with a smaller or larger exponent than in the critical case, respectively (in one-dimensional cases, the couplings would decrease with an exponent different from -1).

ACKNOWLEDGMENTS

We wish to thank O. Giraud for fruitful discussions. This paper has been supported through EUR NanoX Grant No. ANR-17-EURE-0009 in the framework of the ‘‘Programme des Investissements d’Avenir’’; by the French National Research Agency (ANR) Grants No. ANR-17-CE30-0024, No. ANR-18-CE30-0017, and No. ANR-19-CE30-0013; and by the Singapore Ministry of Education Academic Research Fund Tier I (WBS Grant No. R-144-000-437-114). We thank Calcul en Midi-Pyrénées and the National Supercomputing Centre of Singapore for computational resources and assistance.

APPENDIX A: POWER-LAW DECAY OF THE AMPLITUDES OF FLOQUET MATRIX ELEMENTS $|U_{p,p'}|$

In this Appendix, we relate the power-law decay of the amplitudes of Floquet matrix elements $|U_{p,p'}|$ in momentum space with the singularity of the kicked potential $V(q)$ in real space.

We consider the regime $K \ll 1$ and make a first-order expansion in K of the Floquet operator Eq. (4) as

$$U_{pp'} = e^{i\Phi_p} \delta_{pp'} - iK e^{i\Phi_p} \sum_{Q=1}^N F_{pQ} V(2\pi Q/N) F_{Qp'}^{-1}. \tag{A1}$$

Therefore,

$$|U_{pp'}| \simeq K \left| \sum_{Q=1}^N F_{pQ} V(2\pi Q/N) F_{Qp'}^{-1} \right| \tag{A2}$$

for $p \neq p'$. Next, we evaluate the Fourier transform

$$\sum_{Q=1}^N F_{pQ} V(2\pi Q/N) F_{Qp'}^{-1} = \sum_{Q=1}^N \frac{1}{N} e^{2i\pi(p-p')Q/N} V\left(\frac{2\pi Q}{N}\right) \tag{A3}$$

as an integral. Notice that the potential $V(q)$ is symmetric with respect to $q = \pi$; hence,

$$\begin{aligned} & \frac{1}{2\pi} \int_0^{2\pi} V(q) e^{i(p-p')q} dq \\ &= \frac{1}{\pi} \operatorname{Re} \int_0^\pi \ln(q) e^{i(p-p')q} dq \\ & \underset{|p-p'| \rightarrow +\infty}{\sim} \operatorname{Re} \frac{i}{|p-p'|} \sum_{r=0}^\infty c_r (\ln|p-p'|)^{1-r}, \end{aligned} \tag{A4}$$

where the coefficients c_r follow [88]:

$$c_r = (-1)^r \binom{1}{r} \sum_{k=0}^r \binom{r}{k} \left(\frac{\pi i}{2}\right)^{(r-k)}. \tag{A5}$$

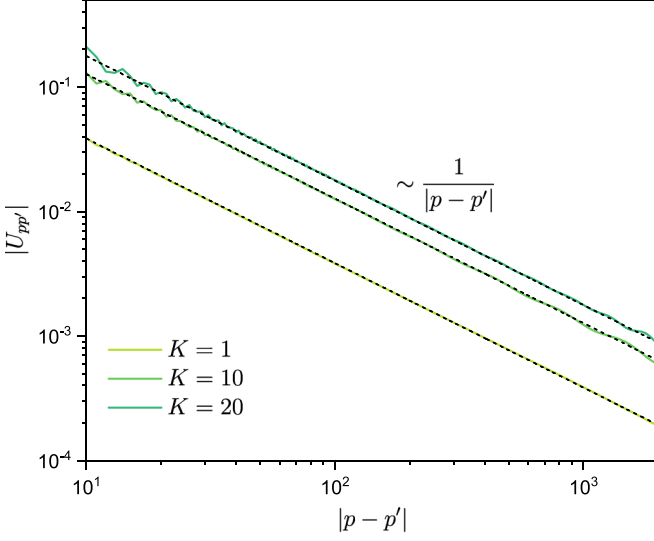


FIG. 9. The decay of off-diagonal matrix elements $|U_{pp'}|$; the dashed lines correspond to Eq. (A6), verifying the conjecture even for large K .

The dominating term is therefore

$$|U_{pp'}| \sim \frac{1}{|p - p'|}. \quad (\text{A6})$$

Note that $V(q)$ has another singularity at $q = \pi$, which is of higher order (first-derivative), compared to the singularity when $q = 0(2\pi)$ (zeroth order); therefore, we only take into account the lowest order.

Although the above arguments are based on a first-order expansion in K valid for $K \ll 1$, numerical data presented in Fig. 9 show that Eq. (A6) is valid even for larger values of K .

APPENDIX B: MULTIFRACTAL PROPERTIES OF THE MKR MODEL

Quantum multifractality can be characterized by the moments P_q [Eq. (1)] of eigenstate amplitudes $|\Psi_\alpha(i)|^2$, $\langle P_q \rangle \sim N^{-\tau_q}$, where $\tau_q = D_q(q - 1)$, D_q are the multifractal dimensions, and N is the system size. Numerically, we compute τ_q by

$$\tau_q(N) = -[\log_2 \langle P_q(N) \rangle - \log_2 \langle P_q(N/2) \rangle]. \quad (\text{B1})$$

The numerical data are shown in Fig. 10 and confirm the multifractal properties of the MKR model, and in particular $D_2 \approx 0.71$.

APPENDIX C: DYNAMICS OF R_0 AND THE MULTIFRACTAL DIMENSIONS

The return probability R_0 can be expressed as $R_0 \equiv |\langle \psi(t) | \psi(0) \rangle|^2$. When starting from a single site j , the initial wave function $|\psi(0)\rangle$ in the eigenbasis $|\phi_k\rangle$ is given by

$$|\psi(0)\rangle = |j\rangle = \sum_k \phi_k(j) |\phi_k\rangle, \quad (\text{C1})$$

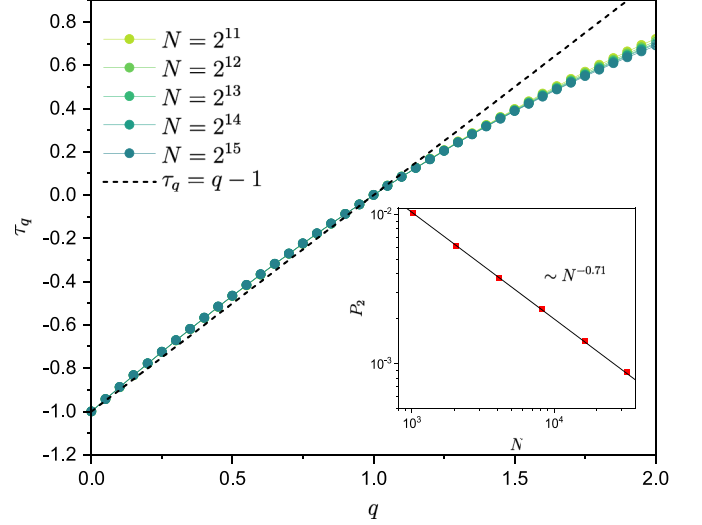


FIG. 10. Multifractal spectrum τ_q of the MKR model for $K = 10$, showing clear deviations from the ergodic behavior. τ_q is determined through Eq. (B1) for different system sizes, from $N = 2^{11}$ to 2^{15} . The data all lie on a single curve, which confirms the algebraic behavior of the eigenstate moments $\langle P_q \rangle$ with N . Inset: Inverse participation ratio $\langle P_2 \rangle \sim N^{-D_2}$ with $D_2 \approx 0.71$. Results have been averaged over 9600 to 38 400 disorder configurations for different system sizes ranging from $N = 2^{15}$ to 2^{11} .

with $\phi_k(j) = \langle \phi_k | j \rangle$, and the evolved wave function at time t is

$$|\psi(t)\rangle = e^{-iE_k t} \sum_k \phi_k(j) |\phi_k\rangle. \quad (\text{C2})$$

Hence, the expression for $R_0(t)$ becomes

$$R_0(t) = \sum_{k,l} e^{-i(E_k - E_l)t} |\phi_k(j)|^2 |\phi_l(j)|^2. \quad (\text{C3})$$

In the limit as t approaches infinity, only the diagonal terms ($k = l$) contribute to the averaging, yielding

$$\langle R_0(t \rightarrow \infty) \rangle = \sum_k |\phi_k(j)|^4 \sim N^{-D_2^\psi}, \quad (\text{C4})$$

where D_2^ψ is defined as the spatial multifractal dimension. In the regime of finite time, the dynamics of R_0 is determined by the off-diagonal elements. Equation (C3) can be rewritten using an integral representation:

$$\begin{aligned} R_0(t) - R_0(\infty) &= \sum_{k \neq l} e^{-i(E_k - E_l)t} |\phi_k(j)|^2 |\phi_l(j)|^2 \\ &= \int d\omega K(\omega, j) e^{-i\omega t}, \end{aligned} \quad (\text{C5})$$

where

$$K(\omega, j) = \rho\left(E + \frac{\omega}{2}; j\right) \rho\left(E - \frac{\omega}{2}; j\right) \quad (\text{C6})$$

represents the correlation of two local densities of states (LDOSs), $\rho(E; j) = \sum_{k=1}^N |\phi_k(j)|^2 \delta(E - E_k)$.

Generally, the properties of the LDOS are influenced by both the eigenstates and the eigenspectrum. In our system, the

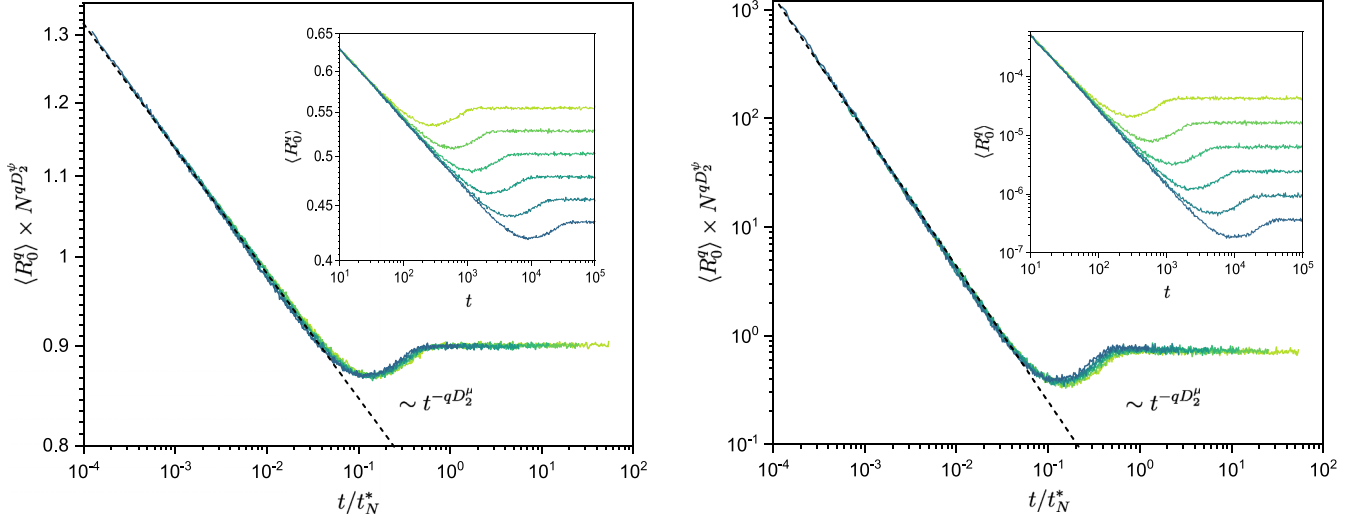


FIG. 11. Scaled $\langle R_0^q \rangle \times N^{qD_2^\psi}$ as a function of the scaled time t/t_N^* for two different q values, $q = 0.1$ for the upper panel and $q = 2$ for the lower one, with the kicked strength $K = 10$. The dashed line represents a fit of the dynamics by $\langle R_0^q \rangle \sim t^{-qD_2^\mu}$. Insets: $\langle R_0^q \rangle$ as a function of time t . Curves from the top to bottom correspond to system sizes $N = 2^{10}, 2^{11}, \dots, 2^{15}$, respectively.

eigenstates exhibit nontrivial multifractal properties characterized by the D_q^ψ dimensions. Similarly, the eigenspectrum can have nontrivial properties, as observed in systems such as the Harper model, the Fibonacci chain, or the Aubry-André model, where the spectrum has a Cantor setlike structure [55,59,65,89]. In such cases, the global density of states $\nu(E) = \frac{1}{N} \sum_{k=1}^N \delta(E - E_k)$ is characterized by a set of multifractal dimensions D_q^0 , as discussed in [89]. This fractal structure of the spectrum contributes to the nontrivial scaling behavior of the LDOS correlation. The fractal dimensions of the LDOS D_q^μ are connected to both the fractal dimension of the eigenstates D_q^ψ and the eigenspectrum D_q^0 , ex-

pressed as $D_2^\mu = D_2^\psi D_{1+D_2^0}$, as demonstrated for the Fibonacci chain [89,90].

The global spectrum of the model we employed is continuous, lacking fractal properties. Therefore, the LDOS inherits nontrivial properties solely from the multifractality of wave functions and we have $D_2^\mu = D_2^\psi$. Nevertheless, such LDOS can be described as a random Cantor set [60].

From the fractal properties of the LDOS, the correlation function $\langle K(\omega) \rangle$, average of $K(\omega, j)$ over the site j and disorder, behaves as shown in previous studies [56,60,87]:

$$\langle K(\omega) \rangle \sim \omega^{1-D_2^\mu}. \tag{C7}$$

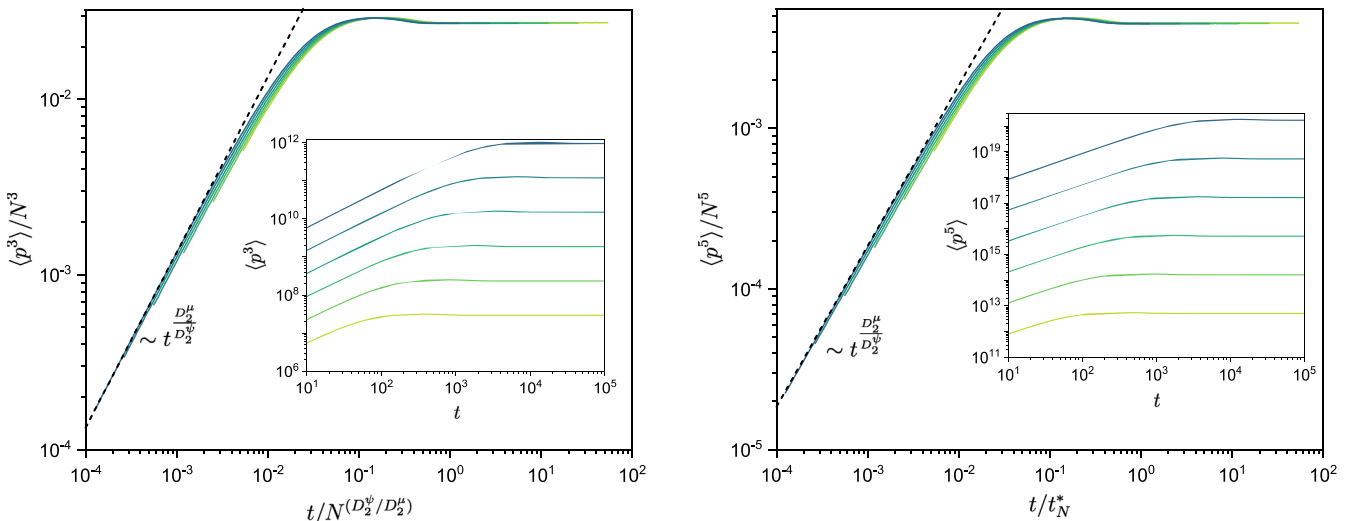


FIG. 12. Scaled moments of the wave packet $\langle p^k \rangle / N^k$ as a function of the scaled time t/t_N^* , for two different values of k , $k = 3$ in the left panel and $k = 5$ in the right panel. The dashed line represents a fit of the dynamics with $\langle p^k \rangle \sim t^{D_2^\mu/D_2^\psi}$. Inset: Moments of the wave packet $\langle p^k \rangle$ as a function of the evolution time t . Curves from bottom to top correspond to system sizes $N = 2^{10}, 2^{11}, \dots, 2^{15}$, respectively.

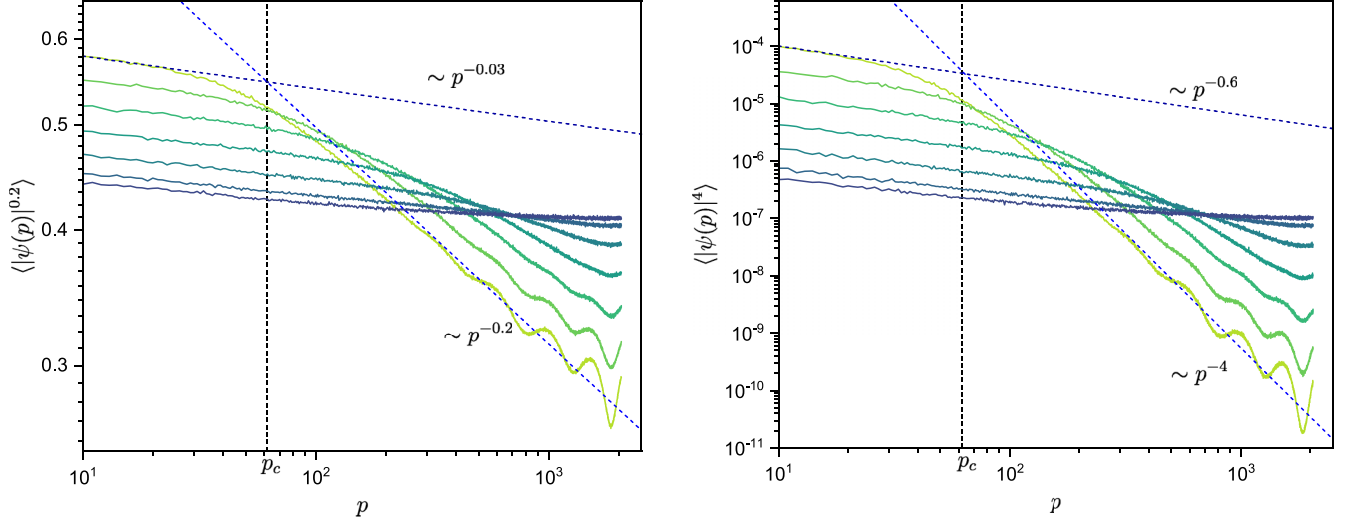


FIG. 13. Averaged probability distribution $\langle |\psi(p, t)|^{2q} \rangle$ at different times for the MKR model with three different values of q , $q = 0.2$ in the left panel and $q = 4$ in the right panel. The dashed lines show the power-law behaviors corresponding to Eq. (10). Curves from top to bottom correspond to increasing time t . Here the kicked strength $K = 10$ and the system size $N = 2^{12}$.

Consequently, employing Eq. (C5), we can deduce the averaged return probability $\langle R_0(t) \rangle$, exhibiting the following scaling behavior:

$$\langle R_0(t) \rangle \sim t^{-D_2^u}. \quad (\text{C8})$$

APPENDIX D: TWO PARAMETER SCALING PROPERTIES OF $\langle R_0^q \rangle$ AND $\langle p^k \rangle$

Figure 11 presents numerical data for $\langle R_0^q \rangle$ of the MKR model [Eq. (2)] for different q values, confirming the validity of the proposed two parameter scaling law Eq. (9).

In Fig. 12, we show numerical data for $\langle p^k \rangle$ for two different $k > 1$ values, showing the universality of the prediction

$\langle p^k \rangle \sim t^{D_2^u/D_2^p}$ and the validity of the proposed scaling laws [Eq. (19)].

APPENDIX E: AVERAGE GENERALIZED WAVE PACKET $\langle |\psi(p, t)|^{2q} \rangle$ FOR DIFFERENT q VALUES AND PROBABILITY DISTRIBUTION OF WAVE FUNCTION AMPLITUDES $|\psi|^2$

Figure 13 presents numerical data for the generalized wave packets $\langle |\psi(p, t)|^{2q} \rangle$, showing the same shape across different q values, in particular the same multifractal wavefront p_c .

In Fig. 14, we present the probability distribution of $\alpha = -\ln |\psi(p, t)|^2 / \ln N$ for different p and t values. On the right

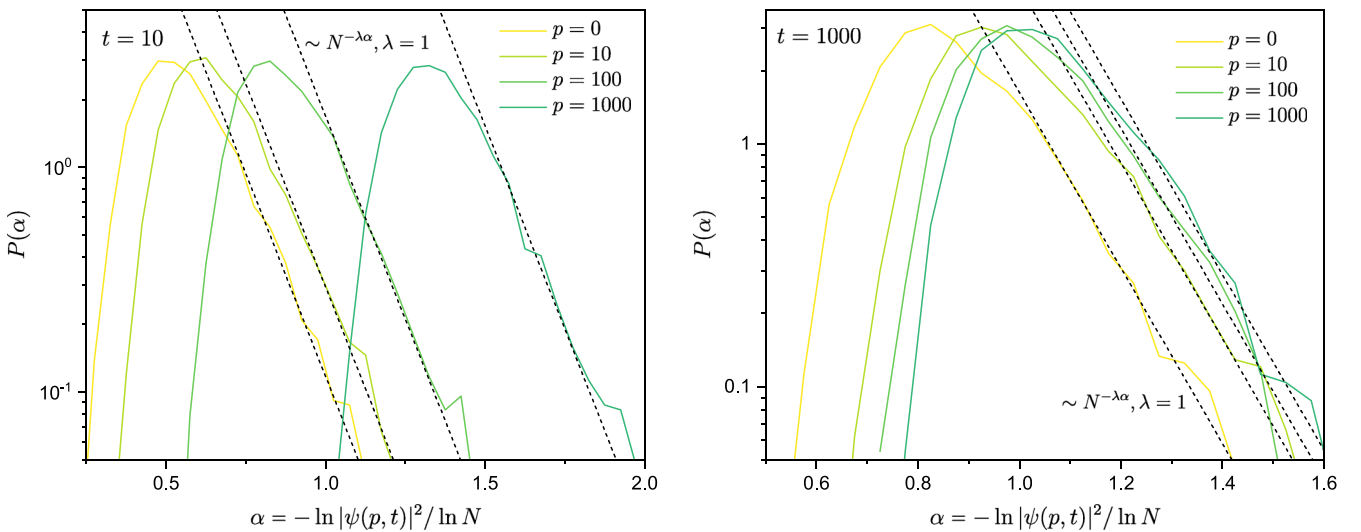


FIG. 14. Probability distributions of $\alpha = -\ln |\psi(p, t)|^2 / \ln N$ for the MKR model at various p values from $p = 0$ to 1000, from right to left. In the left panel, we show data at time $t = 10$, while $t = 1000$ in the right panel. The system size is $N = 2^{12}$. The dashed lines show fits of the exponential tails $P(\alpha) \sim N^{-\lambda\alpha}$ induced by Gaussian fluctuations and responsible for algebraic fat tails of the distribution of wave function amplitudes $|\psi|^2$ at small amplitudes. However, such an exponential tail is absent for small α , i.e., large wave function amplitudes $|\psi|^2$, the regime of interest when calculating positive moments $\langle |\psi(p, t)|^{2q} \rangle$ with $q > 0$.

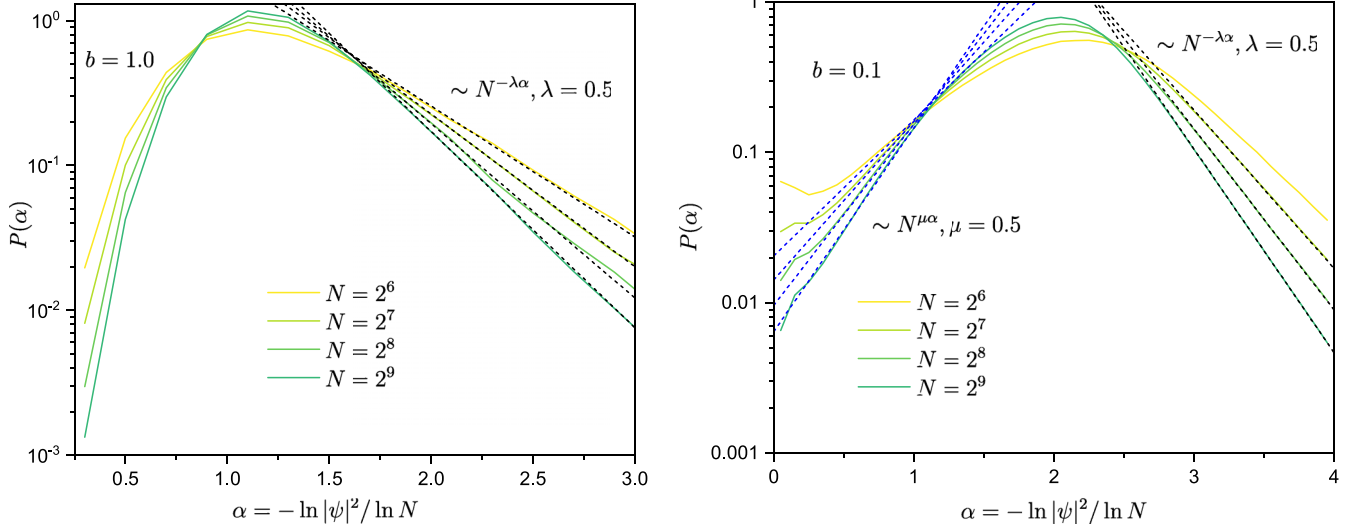


FIG. 15. Probability distributions of $\alpha = -\ln |\psi(p, t)|^2 / \ln N$ for the critical PRBM model [14,15]. The black dashed lines represent fits of the exponential tails $P(\alpha) \sim N^{-\lambda\alpha}$ induced by Gaussian fluctuations and the blue dashed lines represent fits of the exponential tails $P(\alpha) \sim N^{-\mu\alpha}$ due to the algebraic localization effect [50]; such tails break down our assumption that $\langle |\psi(r, t)|^{2q} \rangle \sim \langle |\psi(r, t)|^2 \rangle^q$ and therefore break down the proposed scaling law for $\langle P_q \rangle$.

side of the distribution corresponding to small wave function amplitudes $|\psi|^2$, we observe that there is an anomalously wide distribution $P(\alpha) \sim N^{-\lambda\alpha}$. Such distributions can be related to the Porter-Thomas law $P(\alpha) \sim N^{\beta(1-\alpha)/2} \exp(-\frac{1}{2}\beta N^{1-\alpha})$ as small amplitudes $|\psi(p, t)|^2$ are described by random matrix theory [50,91], where $\beta = 1, 2$ is the Dyson index corresponding to the orthogonal ensemble and unitary ensemble. Hence, when $\alpha \gg 1$ and $N \gg 1$, $P(\alpha) \sim N^{-\lambda\alpha}$ with $\lambda = \beta/2$.

We confirm such scaling behavior of Gaussian fluctuations both in the MKR model ($\beta = 2$) and the critical PRBM model ($\beta = 1$) [14,15] (see Fig. 15).

However, on the left side of the distribution corresponding to large wave function amplitudes $|\psi|^2$, $P(\alpha)$ decreases faster than exponentially, indicating the absence of an algebraic fat for the corresponding distribution of $|\psi(p, t)|^2$ at large amplitudes $|\psi(p, t)|^2$. This absence of large fluctuations at large amplitudes is responsible for $\langle |\psi(p, t)|^{2q} \rangle \sim \langle |\psi(p, t)|^2 \rangle^q$ for $q > 0$. Hence, the shape of $\langle |\psi(p, t)|^{2q} \rangle$ as a function of p is

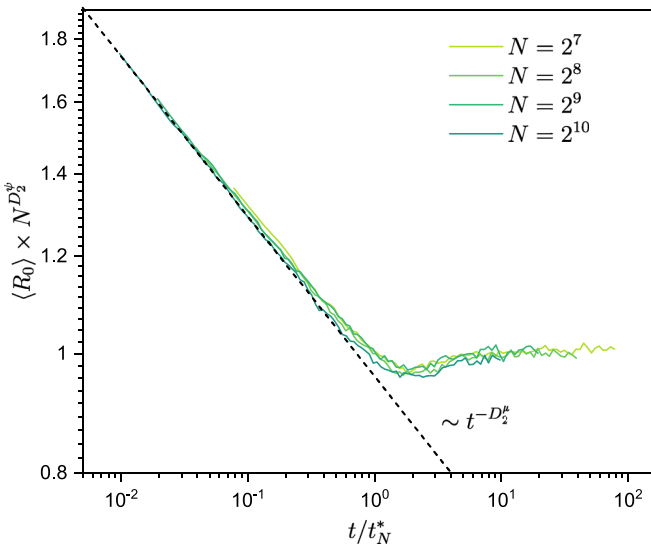


FIG. 16. Demonstration of the scaling property Eq. (9) for the return probability R_0 in the PRBM model Eq. (F1): the data corresponding to different system sizes $N = 2^7, 2^8, \dots, 2^{10}$ and different times $t \in [10, 10^4]$ all collapse onto a single scaling curve when $\langle R_0 \rangle \times N^{D_2^\psi}$ is plotted as a function of the scaled time t/t_N^* . The dashed line indicates a fit by the power law $\langle R_0 \rangle \sim t^{-D_2^\psi}$ with $D_2^\psi \approx D_2^\mu \approx 0.13$. Results have been averaged over 3600 disorder configurations with $b = 0.1$.

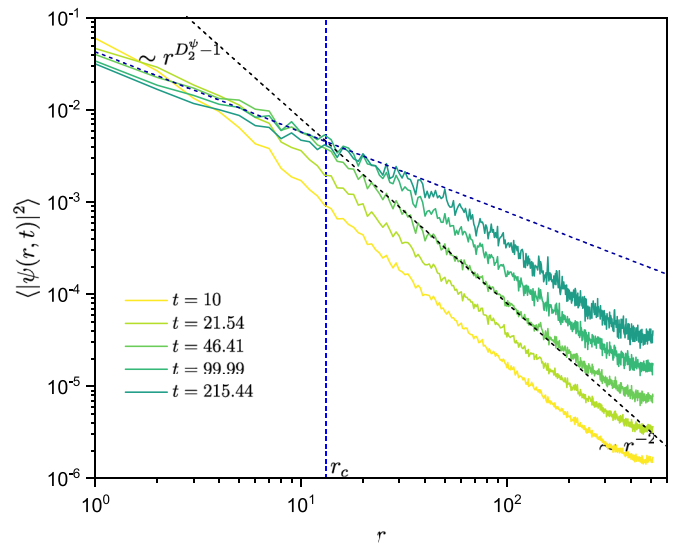


FIG. 17. Average probability distribution of wave packets $\langle |\psi(r, t)|^2 \rangle$ at different times in the PRBM model Eq. (F1) with initial condition $\psi(r, t=0) = \delta_{r,0}$, where we denote $r = |i - j|$. The dashed lines show the two power-law behaviors corresponding to Eq. (10) with $D_2^\psi \approx 0.13$ and the multifractal wavefront r_c . Results have been averaged over 3600 disorder configurations with $b = 0.1$ for system size $N = 2^{10}$.

the same for different $q > 0$ values; in particular they have the same p_c .

APPENDIX F: ADDITIONAL RESULTS FOR THE PRBM MODEL

Here, we present additional results for the wave packet dynamics in the PRBM model [14,15], a paradigmatic model of quantum multifractality [3]. This model consists of $N \times N$ Hermitian matrices \hat{H} with independent Gaussian random variables as matrix elements, where $\langle H_{ij} \rangle = 0$ and the variance is given by

$$\langle |H_{ij}|^2 \rangle = \begin{cases} \beta^{-1}, & i = j, \\ \left[1 + \left(\frac{|i-j|}{b}\right)^2\right]^{-1}, & i \neq j. \end{cases} \quad (\text{F1})$$

Here, $\beta = 1$ for real Hermitian matrices and $\beta = 2$ for complex Hermitian matrices, representing the Dyson indices for the orthogonal class and the unitary class, respectively. In the limit $|i - j| \gg b$, the behavior simplifies to

$$\sqrt{\langle |H_{ij}|^2 \rangle} \simeq \frac{b}{|i - j|}. \quad (\text{F2})$$

This behavior exhibits multifractality and long-range hopping, fundamental features that underlie our wave packet descriptions. We anticipate that the wave packets in this model will exhibit similar behavior as described by Eq. (10).

We conducted numerical simulations for the dynamics of this model using the equation

$$|\psi(t)\rangle = V \exp(-i\Lambda t) V^\dagger |\psi(0)\rangle, \quad (\text{F3})$$

where Λ represents the diagonal matrix of eigenvalues and V is the orthogonal matrix formed by the corresponding eigenstates. The initial state was localized in a single site, defined as $|\psi(t=0)\rangle = |r=0\rangle$. Due to the necessity of exact diagonalization of the Hamiltonian matrix, the system size was considerably limited compared to the Floquet model described in the main text.

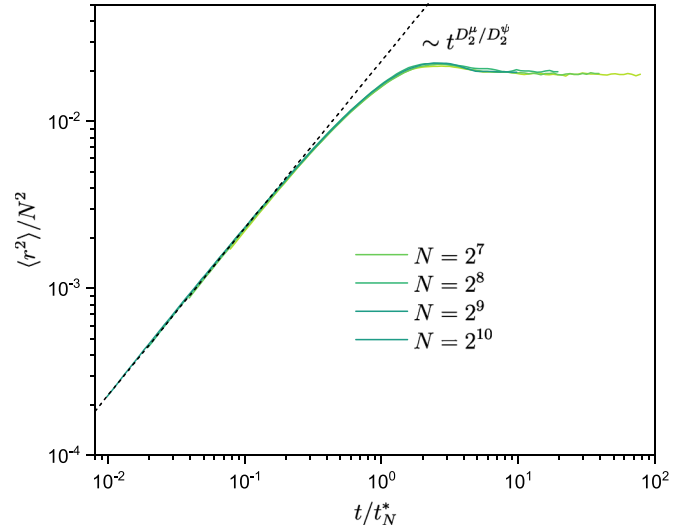


FIG. 18. Demonstration of the scaling property Eq. (19) for the moment of the wave packet $\langle r^2 \rangle$ in the PRBM model Eq. (F1): the data corresponding to different system sizes $N = 2^7, 2^8, \dots, 2^{10}$ and different times $t \in [10, 10^4]$ all collapse onto a single scaling curve when $\langle r^2 \rangle / N^2$ is plotted as a function of the scaled time t/t_N^* . The dashed line indicates a fit by the power law $\langle r^2 \rangle \sim t^{D_2^u/D_2^p}$. Results have been averaged over 3600 disorder configurations with $b = 0.1$.

In Fig. 16, the collapse of $\langle R_0(t) \rangle$ into a single scaling curve when $\langle R_0(t) \rangle N^{D_2^p}$ is plotted against t/t_N^* validates the proposed scaling law [Eq. (9)]. Figure 17 illustrates the averaged probability distribution of the wave packet initialized at $r = 0$, $\langle |\psi(r, t)|^2 \rangle$, at different times, confirming the universality of our model. Additionally, the numerical results presented in Fig. 18 demonstrate that the data for $\langle r^2 \rangle$ in this model conform to the proposed scaling behavior.

However, it is important to note that reproducing the scaling laws for $\langle P_q \rangle$ for the parameter $b = 0.1$ posed challenges. This is due to a nontrivial fat tail in the probability distribution of the wave function amplitudes at $b = 0.1$, resulting in $\langle |\psi(r, t)|^{2a} \rangle \neq \langle |\psi(r, t)|^2 \rangle^a$ (see Fig. 15). This discrepancy breaks down the proposed scaling law for $\langle P_q \rangle$.

[1] S. Sachdev, Quantum phase transitions, *Phys. World* **12**, 33 (1999).
 [2] P. W. Anderson, Absence of diffusion in certain random lattices, *Phys. Rev.* **109**, 1492 (1958).
 [3] F. Evers and A. D. Mirlin, Anderson transitions, *Rev. Mod. Phys.* **80**, 1355 (2008).
 [4] E. Abrahams, *50 Years of Anderson Localization* (World Scientific, Singapore, 2010), Vol. 24.
 [5] B. B. Mandelbrot, Intermittent turbulence in self-similar cascades: Divergence of high moments and dimension of the carrier, *J. Fluid Mech.* **62**, 331 (1974).
 [6] B. B. Mandelbrot and B. B. Mandelbrot, *The Fractal Geometry of Nature* (Freeman, New York, 1982), Vol. 1.
 [7] K. Falconer, *Fractal Geometry: Mathematical Foundations and Applications* (Wiley, New York, 2004).

[8] A. Rodriguez, L. J. Vasquez, and R. A. Römer, Multifractal analysis with the probability density function at the three-dimensional Anderson transition, *Phys. Rev. Lett.* **102**, 106406 (2009).
 [9] S. Faez, A. Strybulevych, J. H. Page, A. Lagendijk, and B. A. van Tiggelen, Observation of multifractality in Anderson localization of ultrasound, *Phys. Rev. Lett.* **103**, 155703 (2009).
 [10] A. Rodriguez, L. J. Vasquez, K. Slevin, and R. A. Römer, Multifractal finite-size scaling and universality at the Anderson transition, *Phys. Rev. B* **84**, 134209 (2011).
 [11] G. Lemarié, J. Chabé, P. Szriftgiser, J. C. Garreau, B. Grémaud, and D. Delande, Observation of the Anderson metal-insulator transition with atomic matter waves: Theory and experiment, *Phys. Rev. A* **80**, 043626 (2009).

- [12] G. Lemarié, H. Lignier, D. Delande, P. Szafrutis, and J. C. Garreau, Critical state of the Anderson transition: Between a metal and an insulator, *Phys. Rev. Lett.* **105**, 090601 (2010).
- [13] J. Chabé, G. Lemarié, B. Grémaud, D. Delande, P. Szafrutis, and J. C. Garreau, Experimental observation of the Anderson metal-insulator transition with atomic matter waves, *Phys. Rev. Lett.* **101**, 255702 (2008).
- [14] A. D. Mirlin, Y. V. Fyodorov, F.-M. Dittes, J. Quezada, and T. H. Seligman, Transition from localized to extended eigenstates in the ensemble of power-law random banded matrices, *Phys. Rev. E* **54**, 3221 (1996).
- [15] A. D. Mirlin and F. Evers, Multifractality and critical fluctuations at the Anderson transition, *Phys. Rev. B* **62**, 7920 (2000).
- [16] A. D. Mirlin, Y. V. Fyodorov, A. Mildnerberger, and F. Evers, Exact relations between multifractal exponents at the Anderson transition, *Phys. Rev. Lett.* **97**, 046803 (2006).
- [17] A. De Luca, B. L. Altshuler, V. E. Kravtsov, and A. Scardicchio, Anderson localization on the Bethe lattice: Nonergodicity of extended states, *Phys. Rev. Lett.* **113**, 046806 (2014).
- [18] V. E. Kravtsov, I. M. Khaymovich, E. Cuevas, and M. Amini, A random matrix model with localization and ergodic transitions, *New J. Phys.* **17**, 122002 (2015).
- [19] N. Macé, F. Alet, and N. Laflorencie, Multifractal scalings across the many-body localization transition, *Phys. Rev. Lett.* **123**, 180601 (2019).
- [20] M. Tarzia, Many-body localization transition in Hilbert space, *Phys. Rev. B* **102**, 014208 (2020).
- [21] G. De Tomasi, I. M. Khaymovich, F. Pollmann, and S. Warzel, Rare thermal bubbles at the many-body localization transition from the Fock space point of view, *Phys. Rev. B* **104**, 024202 (2021).
- [22] G. D. Tomasi, M. Amini, S. Bera, I. M. Khaymovich, and V. E. Kravtsov, Survival probability in Generalized Rosenzweig-Porter random matrix ensemble, *SciPost Phys.* **6**, 014 (2019).
- [23] I. M. Khaymovich, V. E. Kravtsov, B. L. Altshuler, and L. B. Ioffe, Fragile extended phases in the log-normal Rosenzweig-Porter model, *Phys. Rev. Res.* **2**, 043346 (2020).
- [24] P. von Soosten and S. Warzel, Non-ergodic delocalization in the Rosenzweig-Porter model, *Lett. Math. Phys.* **109**, 905 (2019).
- [25] K. Truong and A. Ossipov, Eigenvectors under a generic perturbation: Non-perturbative results from the random matrix approach, *Europhys. Lett.* **116**, 37002 (2016).
- [26] E. Bogomolny and M. Sieber, Eigenfunction distribution for the Rosenzweig-Porter model, *Phys. Rev. E* **98**, 032139 (2018).
- [27] C. Monthus, Multifractality of eigenstates in the delocalized non-ergodic phase of some random matrix models: Wigner-Weisskopf approach, *J. Phys. A* **50**, 295101 (2017).
- [28] M. Amini, Spread of wave packets in disordered hierarchical lattices, *Europhys. Lett.* **117**, 30003 (2017).
- [29] G. Biroli and M. Tarzia, Lévy-Rosenzweig-Porter random matrix ensemble, *Phys. Rev. B* **103**, 104205 (2021).
- [30] V. Kravtsov, I. Khaymovich, B. Altshuler, and L. Ioffe, Localization transition on the random regular graph as an unstable tricritical point in a log-normal Rosenzweig-Porter random matrix ensemble, [arXiv:2002.02979](https://arxiv.org/abs/2002.02979) (2020).
- [31] I. M. Khaymovich and V. E. Kravtsov, Dynamical phases in a “multifractal” Rosenzweig-Porter model, *SciPost Phys.* **11**, 045 (2021).
- [32] K. S. Tikhonov and A. D. Mirlin, Fractality of wave functions on a Cayley tree: Difference between tree and locally treelike graph without boundary, *Phys. Rev. B* **94**, 184203 (2016).
- [33] G. Biroli and M. Tarzia, Delocalization and ergodicity of the Anderson model on Bethe lattices, [arXiv:1810.07545](https://arxiv.org/abs/1810.07545) (2018).
- [34] V. Kravtsov, B. Altshuler, and L. Ioffe, Non-ergodic delocalized phase in Anderson model on Bethe lattice and regular graph, *Ann. Phys. (NY)* **389**, 148 (2018).
- [35] G. Parisi, S. Pascazio, F. Pietracaprina, V. Ros, and A. Scardicchio, Anderson transition on the bethe lattice: an approach with real energies, *J. Phys. A* **53**, 014003 (2020).
- [36] J. N. Bandyopadhyay, J. Wang, and J. Gong, Generating a fractal butterfly Floquet spectrum in a class of driven SU(2) systems: Eigenstate statistics, *Phys. Rev. E* **81**, 066212 (2010).
- [37] S. Ray, A. Ghosh, and S. Sinha, Drive-induced delocalization in the Aubry-André model, *Phys. Rev. E* **97**, 010101(R) (2018).
- [38] M. Sarkar, R. Ghosh, A. Sen, and K. Sengupta, Mobility edge and multifractality in a periodically driven Aubry-André model, *Phys. Rev. B* **103**, 184309 (2021).
- [39] S. Roy, I. M. Khaymovich, A. Das, and R. Moessner, Multifractality without fine-tuning in a Floquet quasiperiodic chain, *SciPost Phys.* **4**, 025 (2018).
- [40] J. Wang, X.-J. Liu, G. Xianlong, and H. Hu, Phase diagram of a non-Abelian Aubry-André-Harper model with p -wave superfluidity, *Phys. Rev. B* **93**, 104504 (2016).
- [41] W. Buijsman and Y. B. Lev, Circular Rosenzweig-Porter random matrix ensemble, *SciPost Phys.* **12**, 082 (2022).
- [42] M. Sarkar, R. Ghosh, and I. Khaymovich, Tuning the phase diagram of a Rosenzweig-Porter model with fractal disorder, *Phys. Rev. B* **108**, L060203 (2023).
- [43] A. Duthie, S. Roy, and D. E. Logan, Anomalous multifractality in quantum chains with strongly correlated disorder, *Phys. Rev. B* **106**, L020201 (2022).
- [44] S. Roy and D. E. Logan, Localization on certain graphs with strongly correlated disorder, *Phys. Rev. Lett.* **125**, 250402 (2020).
- [45] C. Castellani and L. Peliti, Multifractal wavefunction at the localisation threshold, *J. Phys. A* **19**, L429 (1986).
- [46] A. Rodriguez, L. J. Vasquez, K. Slevin, and R. A. Römer, Critical parameters from a generalized multifractal analysis at the Anderson transition, *Phys. Rev. Lett.* **105**, 046403 (2010).
- [47] E. Bogomolny and O. Giraud, Perturbation approach to multifractal dimensions for certain critical random-matrix ensembles, *Phys. Rev. E* **84**, 036212 (2011).
- [48] E. Bogomolny and O. Giraud, Multifractal dimensions for all moments for certain critical random-matrix ensembles in the strong multifractality regime, *Phys. Rev. E* **85**, 046208 (2012).
- [49] E. Cuevas, V. Gasparian, and M. Ortuño, Anomalously large critical regions in power-law random matrix ensembles, *Phys. Rev. Lett.* **87**, 056601 (2001).
- [50] A. M. Bilen, B. Georgeot, O. Giraud, G. Lemarié, and I. García-Mata, Symmetry violation of quantum multifractality: Gaussian fluctuations versus algebraic localization, *Phys. Rev. Res.* **3**, L022023 (2021).
- [51] P. A. Nosov, I. M. Khaymovich, and V. E. Kravtsov, Correlation-induced localization, *Phys. Rev. B* **99**, 104203 (2019).
- [52] T. Ohtsuki and T. Kawarabayashi, Anomalous diffusion at the Anderson transitions, *J. Phys. Soc. Jpn.* **66**, 314 (1997).

- [53] C. A. Müller, D. Delande, and B. Shapiro, Critical dynamics at the Anderson localization mobility edge, *Phys. Rev. A* **94**, 033615 (2016).
- [54] P. Sierant, D. Delande, and J. Zakrzewski, Thouless time analysis of Anderson and many-body localization transitions, *Phys. Rev. Lett.* **124**, 186601 (2020).
- [55] A. Szabó and U. Schneider, Non-power-law universality in one-dimensional quasicrystals, *Phys. Rev. B* **98**, 134201 (2018).
- [56] R. Ketzmerick, G. Petschel, and T. Geisel, Slow decay of temporal correlations in quantum systems with cantor spectra, *Phys. Rev. Lett.* **69**, 695 (1992).
- [57] V. E. Kravtsov, A. Ossipov, O. M. Yevtushenko, and E. Cuevas, Dynamical scaling for critical states: Validity of Chalker's Ansatz for strong fractality, *Phys. Rev. B* **82**, 161102(R) (2010).
- [58] V. E. Kravtsov, A. Ossipov, and O. M. Yevtushenko, Return probability and scaling exponents in the critical random matrix ensemble, *J. Phys. A* **44**, 305003 (2011).
- [59] M. Hopjan and L. Vidmar, Scale-invariant survival probability at eigenstate transitions, *Phys. Rev. Lett.* **131**, 060404 (2023).
- [60] B. L. Altshuler and V. E. Kravtsov, Random Cantor sets and mini-bands in local spectrum of quantum systems, *arXiv:2301.12279* (2023).
- [61] S. Ghosh, C. Miniatura, N. Cherroret, and D. Delande, Coherent forward scattering as a signature of Anderson metal-insulator transitions, *Phys. Rev. A* **95**, 041602(R) (2017).
- [62] M. Martinez, G. Lemarié, B. Georgeot, C. Miniatura, and O. Giraud, Coherent forward scattering as a robust probe of multifractality in critical disordered media, *SciPost Phys.* **14**, 057 (2023).
- [63] P. Akridas-Morel, N. Cherroret, and D. Delande, Multifractality of the kicked rotor at the critical point of the Anderson transition, *Phys. Rev. A* **100**, 043612 (2019).
- [64] M. Martinez, G. Lemarié, B. Georgeot, C. Miniatura, and O. Giraud, Coherent forward scattering peak and multifractality, *Phys. Rev. Res.* **3**, L032044 (2021).
- [65] R. Ketzmerick, K. Kruse, S. Kraut, and T. Geisel, What determines the spreading of a wave packet?, *Phys. Rev. Lett.* **79**, 1959 (1997).
- [66] I. García-Mata, J. Martin, O. Giraud, and B. Georgeot, Multifractality of quantum wave packets, *Phys. Rev. E* **86**, 056215 (2012).
- [67] V. E. Kravtsov, O. M. Yevtushenko, P. Snajberk, and E. Cuevas, Lévy flights and multifractality in quantum critical diffusion and in classical random walks on fractals, *Phys. Rev. E* **86**, 021136 (2012).
- [68] R. P. A. Lima, F. A. B. F. de Moura, M. L. Lyra, and H. N. Nazareno, Critical wave-packet dynamics in the power-law bond disordered Anderson model, *Phys. Rev. B* **71**, 235112 (2005).
- [69] M. Santhanam, S. Paul, and J. B. Kannan, Quantum kicked rotor and its variants: Chaos, localization and beyond, *Phys. Rep.* **956**, 1 (2022).
- [70] B. V. Chirikov, A universal instability of many-dimensional oscillator systems, *Phys. Rep.* **52**, 263 (1979).
- [71] F. M. Izrailev, Simple models of quantum chaos: Spectrum and eigenfunctions, *Phys. Rep.* **196**, 299 (1990).
- [72] D. V. Else, B. Bauer, and C. Nayak, Floquet time crystals, *Phys. Rev. Lett.* **117**, 090402 (2016).
- [73] A. M. García-García and J. Wang, Anderson transition in quantum chaos, *Phys. Rev. Lett.* **94**, 244102 (2005).
- [74] I. García-Mata, J. Martin, R. Dubertrand, O. Giraud, B. Georgeot, and G. Lemarié, Two critical localization lengths in the Anderson transition on random graphs, *Phys. Rev. Res.* **2**, 012020(R) (2020).
- [75] S. Bera, G. De Tomasi, I. M. Khaymovich, and A. Scardicchio, Return probability for the Anderson model on the random regular graph, *Phys. Rev. B* **98**, 134205 (2018).
- [76] K. S. Tikhonov and A. D. Mirlin, Many-body localization transition with power-law interactions: Statistics of eigenstates, *Phys. Rev. B* **97**, 214205 (2018).
- [77] R. Modak and T. Nag, Many-body dynamics in long-range hopping models in the presence of correlated and uncorrelated disorder, *Phys. Rev. Res.* **2**, 012074(R) (2020).
- [78] R. Modak and T. Nag, Many-body localization in a long-range model: Real-space renormalization-group study, *Phys. Rev. E* **101**, 052108 (2020).
- [79] G. Lemarié, C. A. Müller, D. Guéry-Odelin, and C. Miniatura, Coherent backscattering and forward-scattering peaks in the quantum kicked rotor, *Phys. Rev. A* **95**, 043626 (2017).
- [80] C. Hainaut, I. Manai, R. Chicireanu, J.-F. Clément, S. Zemmouri, J. C. Garreau, P. Szriftgiser, G. Lemarié, N. Cherroret, and D. Delande, Return to the origin as a probe of atomic phase coherence, *Phys. Rev. Lett.* **118**, 184101 (2017).
- [81] S. Fishman, D. R. Grempel, and R. E. Prange, Chaos, quantum recurrences, and Anderson localization, *Phys. Rev. Lett.* **49**, 509 (1982).
- [82] G. D. Birkhoff, Proof of the ergodic theorem, *Proc. Natl. Acad. Sci. USA* **17**, 656 (1931).
- [83] D. R. Grempel, R. E. Prange, and S. Fishman, Quantum dynamics of a nonintegrable system, *Phys. Rev. A* **29**, 1639 (1984).
- [84] O. Giraud, J. Marklof, and S. O'Keefe, Intermediate statistics in quantum maps, *J. Phys. A* **37**, L303 (2004).
- [85] J. T. Chalker and G. J. Daniell, Scaling, diffusion, and the integer quantized Hall effect, *Phys. Rev. Lett.* **61**, 593 (1988).
- [86] J. Chalker, Scaling and eigenfunction correlations near a mobility edge, *Physica A* **167**, 253 (1990).
- [87] E. Cuevas and V. E. Kravtsov, Two-eigenfunction correlation in a multifractal metal and insulator, *Phys. Rev. B* **76**, 235119 (2007).
- [88] R. Wong and J. Lin, Asymptotic expansions of fourier transforms of functions with logarithmic singularities, *J. Math. Anal. Appl.* **64**, 173 (1978).
- [89] N. Macé, A. Jagannathan, and F. Piéchon, Fractal dimensions of wave functions and local spectral measures on the fibonacci chain, *Phys. Rev. B* **93**, 205153 (2016).
- [90] M. Reisner, Y. Tahmi, F. Piéchon, U. Kuhl, and F. Mortessagne, Experimental observation of multifractality in fibonacci chains, *Phys. Rev. B* **108**, 064210 (2023).
- [91] C. E. Porter and R. G. Thomas, Fluctuations of nuclear reaction widths, *Phys. Rev.* **104**, 483 (1956).